Experimental Realization of Two Decoupled Directional Couplers in a Subwavelength Packing by Adiabatic Elimination

Michael Mrejen,[†,‡] Haim Suchowski,[†] Taiki Hatakeyama,[†] Yuan Wang,[†] and Xiang Zhang[*,†,§,⊥]

[†]NSF Nanoscale Science and Engineering Center (NSEC) and [‡]Graduate Group in Applied Science and Technology, University of California, Berkeley, Berkeley, California 94720, United States

[§]Materials Sciences Division, Lawrence Berkeley National Laboratory, 1 Cyclotron Road, Berkeley, California 94720, United States

[⊥]Department of Physics, King Abdulaziz University, Jeddah, 21589, Saudi Arabia

ABSTRACT: On-chip optical data processing and photonic quantum integrated circuits require the integration of densely packed directional couplers at the nanoscale. However, the inherent evanescent coupling at this length scale severely limits the compactness of such on-chip photonic circuits. Here, inspired by the adiabatic elimination in a N-level atomic system, we report an experimental realization of a pair of directional couplers that are effectively isolated from each other despite their subwavelength packing. This approach opens the way to ultradense arrays of waveguide couplers for integrated optical and quantum logic gates.

KEYWORDS: Integrated optics devices, waveguides, quantum computing, nanophotonics, atomic molecular and optical physics, near-field optical microscopy
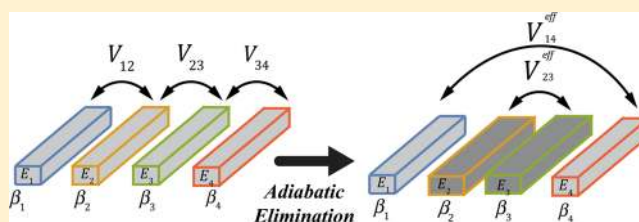
The directional couplers,[1] two interacting optical waveguides placed in close proximity, are a cornerstone in integrated photonic circuits and are widely used in devices such as optical modulators and switches for high-speed communication and on-chip data processing.[2−4] More recently, the directional coupler has been harnessed as the building block for photonic quantum integrated circuits and shown to enable quantum computing logic operations when used with single photons.[5−8]

Typically, the directional couplers are used to split optical power in an integrated format as beamsplitters for free space propagation. This operation is achieved by coupling the two waveguides when they are brought sufficiently close together so that the evanescent fields of the guided modes overlap. However, a closely packed arrangement of those couplers results in undesirable cross-talk between them, due to the evanescent coupling, thus severely limiting the compactness of on-chip optical data processing and photonic quantum integrated circuits, which require at least a pair of directional couplers to achieve their functionality. For instance, Politi et al.[5] have shown the realization of a complex quantum logic gate with the integration of pairs of directional couplers. However, each coupler has an inversion length of several millimeters and a footprint of at least 10 μm in the lateral dimension. These dimension constraints therefore result in large devices when integrating several such quantum logic gates required for quantum computing. In this work, inspired by the adiabatic elimination (AE) in a N-level atomic system, we report an experimental realization of a pair of directional couplers that are effectively isolated from each other despite their subwavelength

packing, therefore overcoming the severe limitation on the density imposed by the evanescent coupling.

The fundamental wave nature of quantum mechanics and optics has allowed the observation at a macroscopic level of optical analogues of quantum phenomena typical to atomic and molecular systems in recent years.[9−15] These analogies provide a powerful and accessible laboratory platform for a direct observation and manipulation of some basic dynamics typically found in two-level or three-level atomic and molecular systems that interact coherently with laser fields.[16−20]

In this Letter, we report on the experimental realization of AE decomposition in a four-waveguides system where the waveguides are packed at the wavelength scale. The AE concept from atomic physics, which decomposes a three-level system into an effective two-level system and a dark state ("2 + 1 decomposition"),[20−23] is employed here to achieve a "2 + 2" decomposition among a four-waveguide coupled system. We show that the AE in this configuration decomposes the four-waveguide system into two decoupled two-waveguide couplers despite the strong coupling. This decomposition follows the N-levels generalized AE[21,24−26] and opens up possibilities of manipulation of classical and quantum light in very compact integrated photonic circuits.

We start our analysis with the description of the propagation of the monochromatic light fields in four coupled waveguides as shown in Figure 1 using the standard coupled mode equations (CMEs):[1,27,28]
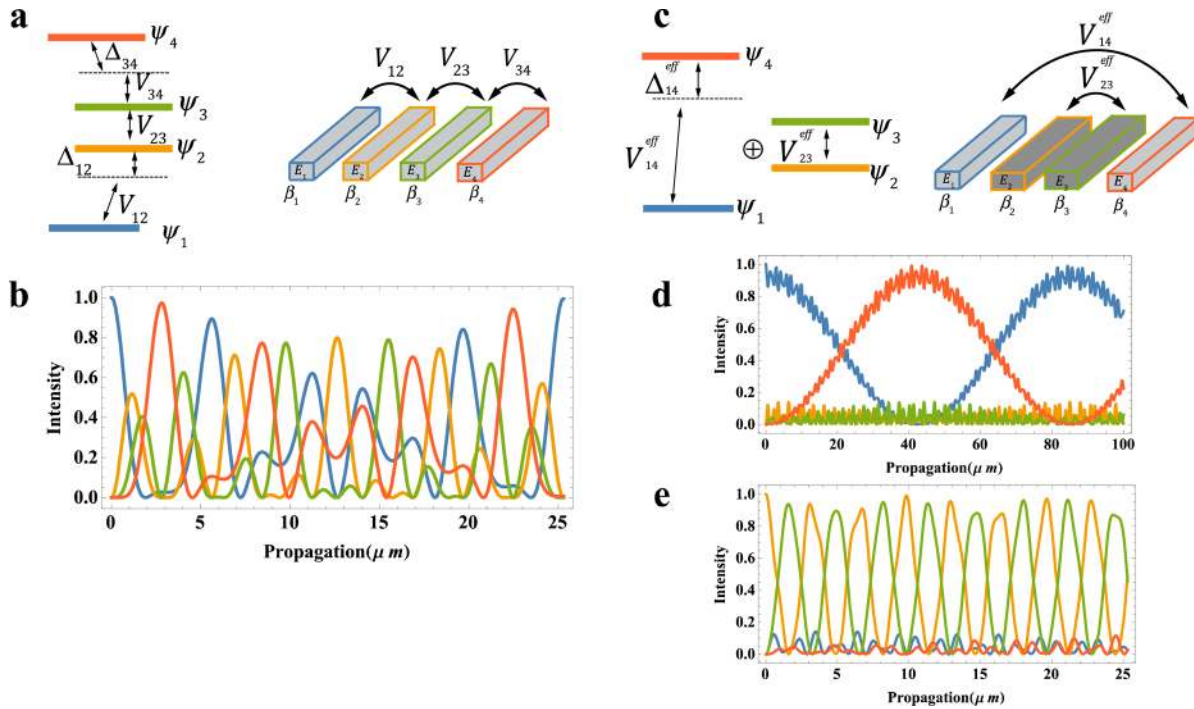
Figure 1. Symmetrical (a, b) versus AE evolution (c−e) in atomic physics and four-waveguide configurations. The color code represents the probability amplitudes of the levels in the atomic case or the field strength in each waveguide. The light is initially injected in waveguide 1 (blue curve). In all cases, the dynamics are dictated by the couplings and the detuning/mode indices via the CMEs (eq 1). (a, b) Symmetrical four-mode dynamics, all modes are excited. (c−e) AE dynamics. The system is decomposed to "2 + 2", effective (d) two-mode coupler on outer waveguides and (e) two-mode coupler of inner waveguide.

$$\frac{d}{dz}\begin{pmatrix} A_1 \\ A_2 \\ A_3 \\ A_4 \end{pmatrix} = i \begin{pmatrix} \beta_1 & V_{12} & 0 & 0 \\ V_{12} & \beta_2 & V_{23} & 0 \\ 0 & V_{23} & \beta_3 & V_{34} \\ 0 & 0 & V_{34} & \beta_4 \end{pmatrix} \begin{pmatrix} A_1 \\ A_2 \\ A_3 \\ A_4 \end{pmatrix}$$

(1)

where z is the propagation direction, and A_i, $i = 1,...,4$, represent the fields of mode i. Each mode is characterized by its propagation constant β_i, and V_{12}, V_{23}, and V_{34} are the couplings strengths between modes 1−2, 2−3, and 3−4, respectively. In our analysis, we have further assumed, without loss of generality, that the outermost waveguides (1,4) and innermost (2,3) are separately identical, thus yielding $\beta_1 = \beta_4$, $\beta_2 = \beta_3$. Finally, we are taking V_{12} and V_{34} to be equal.

The CMEs (eq 1) are analogous to the four-level atomic system depicted in Figure 1, where laser fields interact near resonance in the transitions $|\Psi_1\rangle \rightarrow |\Psi_2\rangle$, $|\Psi_3\rangle \rightarrow |\Psi_4\rangle$ and on-resonance in the transition $|\Psi_2\rangle \rightarrow |\Psi_3\rangle$. In this analogy, the time evolution of the population of electrons in each level of the atomic system is equivalent to the propagation in space of the light in each waveguide. In both cases, the evolution is dictated by the couplings between the modes V_{ij} and by the detuning between the levels Δ_{ij} or propagation constants differences $\Delta\beta_{ij} = \beta_j - \beta_i$. Such coupled system typically exhibits a dynamics where all the coupled modes or levels are "populated". As we show in Figure 1, panel a, this is particularly the case in the waveguide system where all the waveguides are identical (note that the couplings $V_{12} = V_{34}$, V_{23} are not necessarily equal). We see that light injected in waveguide 1 (light blue curve) oscillates between all the four waveguides as it propagates. However, applying the AE constraint on the system, namely that adjacent and detuned modes or levels are strongly detuned and coupled or $\Delta\beta_{12}$, $\Delta\beta_{34} \gg V_{12}$, V_{34} allows

to decompose the dynamics of the system into a 2 + 2 dynamical space where the pairs of outermost waveguides and innermost waveguides constitute each a standalone two-waveguide coupler. This 2 + 2 decomposition is clearly apparent in Figure 1, panel b where we solve eq 1 under the mentioned conditions. We first considered the system with light injected in waveguide 1. We see that the energy oscillates primarily between the outermost waveguides (1 and 4, light blue and dark orange curves, respectively), whereas at waveguides 2,3 and accumulates virtually no energy. Since each of the two outer coupling processes is greatly mismatched to the inner waveguides, the amplitude of the middle waveguides A_2, A_3, oscillates very rapidly in comparison to the slow varying amplitudes A_1, A_4. Here resides the adiabaticity of the AE, where the rapidly varying variables of the system (A_2, A_3) must follow the adiabatically slow varying variables (A_1, A_4) and are thus eliminated.[24,26] As a result, the amplitude of the intermediate waveguides cannot build up significantly and thus remains at the initial value. This occurs despite the two inner waveguides being identical with no mode index mismatch between them. However, when the initial condition is changed to the injection in one of the inner waveguides, the situation is reversed. As expected from the AE decomposition, the inner waveguides form an effective two-waveguide system that evolves with light oscillating only between inner waveguides 2 and 3.

A band diagram approach gives a direct visualization of this 2 + 2 AE decomposition. Such band diagram is presented in Figure 2, panel a. The diagram shows the four eigen values of the CMEs (eq 1) as a function of the detuning $\Delta\beta_{12} = \Delta\beta_{34} = \Delta\beta$. We clearly see that as we vary the detuning $\Delta\beta$, the four branches of the diagram separate into two sets of branches. A look at the eigen vectors that constitute each branch reveals
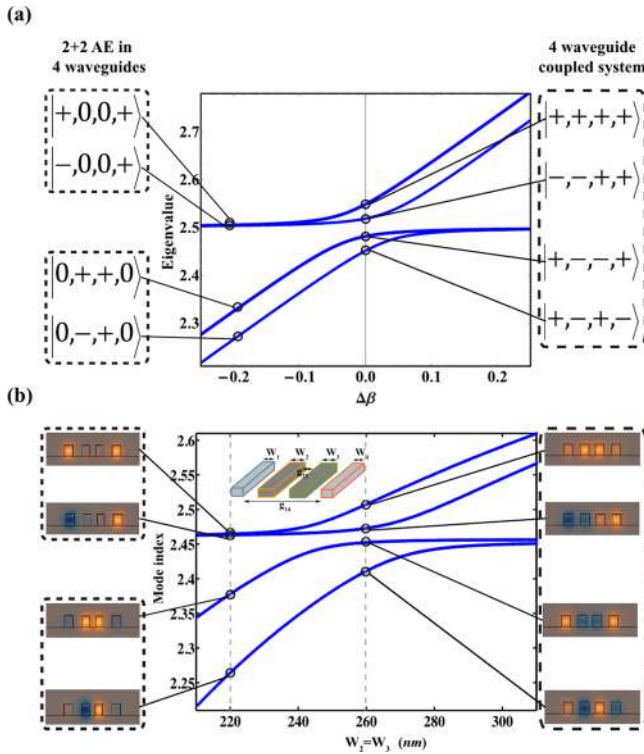
Figure 2. Band diagrams of the four-waveguide system (a) as a function of the mode index difference, $\Delta\beta$, and (b) as a function of the inner waveguides' widths $w_2 = w_3$. The associated eigenmode field profiles and eigen vectors are presented on the left and right column. When $\Delta\beta = 0$, $w_1 = w_2 = w_3 = w_4$, all the eigenmodes are coupled and bunched together (right column), and all the mode profiles are shown to be a superposition of all the waveguides (bare basis vectors). The bands split to clearly bunch into two sets of bands when the detuning significantly exceeds the couplings (the AE condition). We observe the AE 2 + 2 decomposition in which the eigenmodes bunched (i.e., coupled) together are symmetric and antisymmetric combinations of only either the outer waveguides or inner waveguides. We note the very good agreement between the analytical solution of the CME and the full wave simulation.

coupling between the modes and are selected to be particularly narrow to ensure a strong coupling as required from the AE constraints. The wavelength is selected to be to be 1310 nm for experimental convenience. The modes forming each branch show that indeed the branches bunched together in the AE regime exhibit symmetric and antisymmetric modes localized only in either the outer waveguides or the inner waveguides. For our experiment, we choose to work deep in the AE elimination regime with $w_2 = w_3 = 220$ nm $< w_1 = w_4$ to ensure a significant overlap of the guided mode and thus a strong evanescent coupling. Here, the widths of the waveguides are selected to support only the fundamental mode in TM polarization. However, the scheme discussed here holds also for TE polarization.

Finally, we note the slight deviation between the analytical model Figure 2, panel a and the full-wave simulation Figure 2, panel b when the detuning becomes very large. This is due to the breaking of the assumption that the couplings remain constant. As we vary the inner widths, the field evanescent tail from the inner waveguides increases, ultimately impacting the mode overlap and thus changing the coupling. We see however that the 2 + 2 AE decomposition still holds even when this assumption breaks.

The silicon waveguides were fabricated using a silicon-on-insulator (SOI) substrate. The thicknesses of silicon and buried oxide were 340 nm and 1 μm, respectively. A 160 nm-thick hydrogen silsesquioxane (HSQ) resist (Dow Corning XR-1541) was spun on the SOI substrate. The HSQ layer was patterned by electron-beam lithography for the etching mask. The silicon waveguides were formed by reactive ion etching in $Cl_2/HBr/O_2$. A 10:1 buffered HF was used to remove the HSQ mask.
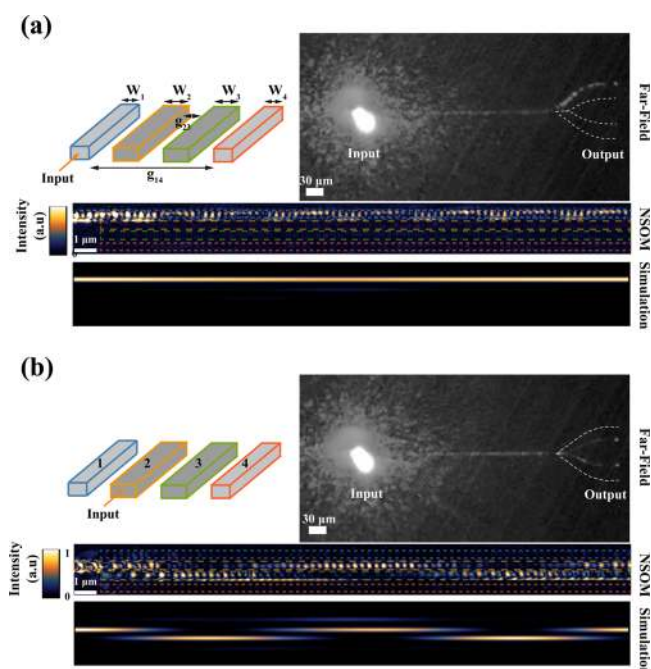
The length of the waveguides in the coupled region is of $L = 250$ μm, and light is injected into either waveguide 1 (outer waveguide) or waveguide 2 (inner waveguide) by the mean of a grating coupler designed to allow efficient coupling into the TM fundamental mode at 1310 nm.[29,30]

The light propagation in the waveguides was examined both in far-field and near-field as described further.

The far-field measurements were carried out on a microscope with a X10/NA 0.3 objective in reflection mode. The light from a continuous wave laser diode at 1310 nm is focused on the input grating. The output lights from the output grating at the end of each waveguide are acquired in reflection mode and imaged on an uncooled infrared focal plane array (IR FPA, Goodrich). The waveguides roughness scatters the coupled light along the propagation and serves as an indication of proper coupling.[31]

The near-field scanning optical microscopy (NSOM) images are acquired using a home-built scattering near-field optical microscope (s-NSOM)[32] in a transmission configuration. In this setup, light from a CW laser diode at 1310 nm is focused on the input grating using a X10/NA 0.3 objective. To ease the alignments, we used a platinum−iridium (PtIr) coated advanced tip at the end of cantilever (ATEC) with a tip radius of 10 nm and tapping frequency of Ω ~300 kHz. The ATEC was moved along the waveguides with subnanometre precision using piezostages to record the propagation of the input light. Light scattered from and modulated by the tip was collected using an aspheric lens (NA = 0.16) and focused onto a 10-MHz InGaAs photoreceiver (NewFocus 2053-FS). The signal was demodulated at 3Ω to filter out the non-near-field background scattering.

The results for the AE case are gathered in Figure 3. We clearly observe the 2 + 2 decomposition as predicted from both

that, while in the on-resonance case, that is, $\Delta\beta = 0$, all the eigenvectors encompass all the modes, the branches bunched together under detuning exhibit symmetric and antisymmetric eigenvectors localized only in either the outer modes or the intermediate ones. As we vary $\Delta\beta$ while the different couplings remain unchanged, we gradually enter the AE regime where $\Delta\beta \gg V_{12}, V_{34}$. This leads to the emergence of two decoupled two-modes dynamics, each one evolving with its own oscillation frequency inversely proportional to the difference between the eigenvalues of the symmetric and antisymmetric modes.

This behavior apparent from the CMEs and the band diagram is further confirmed experimentally. We design our sample using the band diagram approach introduced earlier. Such band diagram is presented in Figure 2, panel b where the eigenmodes are found using the eigenfrequency solver of COMSOL. With a striking agreement with the coupled mode model, here also the diagram shows the four branches separating into two sets of branches as we vary $w_2 = w_3$, that is, the detuning between the inner and outer waveguides. All the geometrical parameters but w_2, w_3 are fixed in accordance with our assumptions and to satisfy the AE constraints and are namely, $g_{23} = 180$ nm, $g_{14} = 1150$ nm, $w_1 = w_4 = 260$ nm. The gaps between the waveguides dictate the strength of the evanescent

Figure 3. Experimental observation of AE in four coupled waveguides. Far-field and NSOM measurements compared to numerical simulations. The AE 2 + 2 decomposition is observed (a) when light is coupled to the outer waveguides and (b) when the light is coupled to the inner ones.

Figure 4. Control experiments on four-symmetrical waveguides, with all waveguides' widths equal. Light oscillates between all the waveguides whether light is coupled to (a) the outer waveguide 1 or to (b) the inner waveguide 2.

the CMEs and the band diagram. We observe in the far field that light injected in waveguide 2 exits the system only from waveguide 2 and 3. The optical near reveals that indeed light oscillates between waveguide 2 and 3 with virtually no leakage to the outer waveguides (1 and 4). In contrast, when light is injected into the outer waveguide (1), the far-field shows it exits the system only from waveguide 1. The NSOM measurement confirms the propagating light is localized in waveguide 1. This is expected since the inversion length predicted by the $L_{inv} = (\lambda/2\Delta n_{14})$ is on the order of 700 μm, well beyond the 250 μm propagation constrained by our e-beam lithography field of view. Those results are in excellent agreement with our propagation simulations based on the eigenmode expansion method (EME)[33] shown in Figure 3.

The dynamics observed are compared to the control case where $w_1 = w_2 = w_3 = w_4 = 260$ nm presented in Figure 4. This comparison shows a stark difference in the evolution with the AE dynamics. We see that, whether the input is in the outer or inner waveguide, all the four outputs show a sizable amount of signal in the far-field measurement. We observe in the near-field that indeed the input light rapidly leaks to all the waveguides and oscillates between them as it propagates. Here also the EME simulations show excellent agreement with the near-field measurements. We note that the AE 2 + 2 decomposition observed here may indicate the possibility of total signal isolation in waveguides arrays with more than three waveguides.[23]

To conclude, we have shown that by employing the AE decomposition in an ultradense four-waveguide system, two isolated two-waveguide couplers with a lateral footprint on the wavelength scale can be obtained. We see that the richness of the system, with its many degrees of freedom, allows a flexible control of the effective couplings in the isolated systems so that each coupler can be designed with its own splitting ratio.
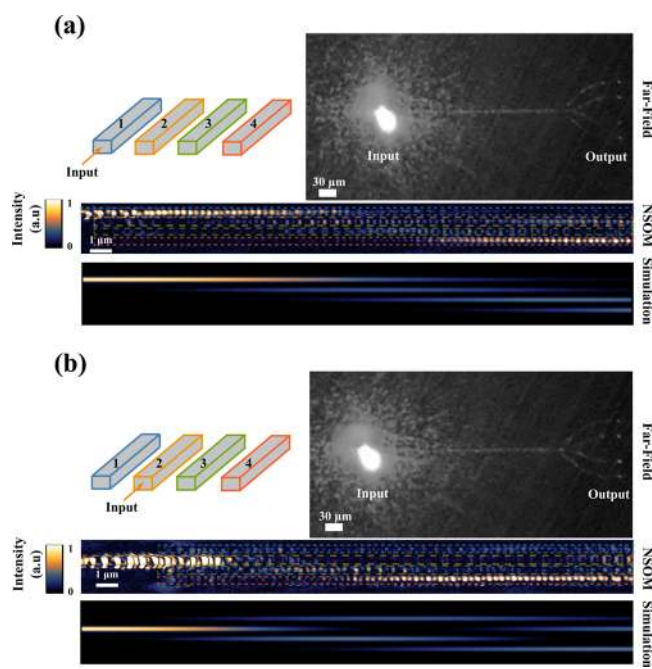
We note also that this approach being inspired from the atomic N-level AE it is foreseen to be generalized to N coupled waveguides opening the way to ultradense arrays of waveguide couplers for integrated optical and quantum logic gates.

■ AUTHOR INFORMATION

Corresponding Author
*E-mail: xiang@berkeley.edu.

Notes
The authors declare no competing financial interest.

■ REFERENCES

(1) Yariv, A. *IEEE J. Quantum Electron.* **1973**, *9*, 919−933.
(2) Green, W. M.; Rooks, M. J.; Sekaric, L.; Vlasov, Y. A. *Opt. Express* **2007**, *15*, 17106−17113.
(3) Xu, Q.; Schmidt, B.; Pradhan, S.; Lipson, M. *Nature* **2005**, *435*, 325−327.
(4) Reed, G. T.; Mashanovich, G.; Gardes, F. Y.; Thomson, D. J. *Nat. Photonics* **2010**, *4*, 518−526.
(5) Politi, A.; Cryan, M. J.; Rarity, J. G.; Yu, S.; O'Brien, J. L. *Science* **2008**, *320*, 646−649.
(6) Peruzzo, A.; Lobino, M.; Matthews, J. C. F.; Matsuda, N.; Politi, A.; Poulios, K.; Zhou, X.-Q.; Lahini, Y.; Ismail, N.; Wörhoff, K.; et al. *Science* **2010**, *329*, 1500−1503.
(7) Peruzzo, A.; Shadbolt, P.; Brunner, N.; Popescu, S.; O'Brien, J. L. *Science* **2012**, *338*, 634−637.
(8) Jian, F.; Shao-Fang, T. *Chin. Phys. Lett.* **2003**, *20*, 1426−1429.
(9) Dragoman, D.; Dragoman, M. *Quantum-Classical Analogies*; Springer: Berlin, Heidelberg, 2004.
(10) Morandotti, R.; Peschel, U.; Aitchison, J. S.; Eisenberg, H. S.; Silberberg, Y. *Phys. Rev. Lett.* **1999**, *83*, 4756−4759.

(11) Christodoulides, D. N.; Lederer, F.; Silberberg, Y. *Nature* **2003**, *424*, 817−823.

(12) Trompeter, H.; Pertsch, T.; Lederer, F.; Michaelis, D.; Streppel, U.; Bräuer, A.; Peschel, U. *Phys. Rev. Lett.* **2006**, *96*, 023901.

(13) Ghulinyan, M.; Oton, C. J.; Gaburro, Z.; Pavesi, L.; Toninelli, C.; Wiersma, D. S. *Phys. Rev. Lett.* **2005**, *94*, 127401.

(14) Longhi, S.; Marangoni, M.; Janner, D.; Ramponi, R.; Laporta, P.; Cianci, E.; Foglietti, V. *Phys. Rev. Lett.* **2005**, *94*, 073002.

(15) Schwartz, T.; Bartal, G.; Fishman, S.; Segev, M. *Nature* **2007**, *446*, 52−55.

(16) Lahini, Y.; Pozzi, F.; Sorel, M.; Morandotti, R.; Silberberg, Y. *Nonlinear Photonics* **2007**, JWBPDP1.

(17) Longhi, S.; Marangoni, M.; Janner, D.; Ramponi, R.; Laporta, P.; Cianci, E.; Foglietti, V. *Phys. Rev. Lett.* **2005**, *94*, 073002.

(18) Ciret, C.; Coda, V.; Rangelov, A. A.; Neshev, D. N.; Montemezzani, G. *Phys. Rev. A: At., Mol., Opt. Phys.* **2013**, *87*, 013806.

(19) Kalonakis, K.; Paspalakis, E. *J. Mod. Opt.* **2005**, *52*, 1885−1892.

(20) Vitanov, N. V.; Halfmann, T.; Shore, B. W.; Bergmann, K. *Annu. Rev. Phys. Chem.* **2001**, *52*, 763−809.

(21) Tannor, D. *Introduction to Quantum Mechanics: A Time-Dependent Perspective*; University Science Book: Sausalito, 2006.

(22) Brion, E.; Pedersen, L. H.; Mølmer, K. *J. Phys. A: Math. Theor.* **2007**, *40*, 1033−1043.

(23) Mrejen, M.; Suchowski, H.; Hatakeyama, T.; Wu, C.; Feng, L.; O'Brien, K.; Wang, Y.; Zhang, X. *Nat. Commun.* **2015**, *6*, 7565.

(24) Lugiato, L.; Prati, F.; Brambilla, M. *Nonlinear Optical Systems*; Cambridge University Press: Cambridge, 2015; pp 105−111.

(25) Vitanov, N. V.; Stenholm, S. *Phys. Rev. A: At., Mol., Opt. Phys.* **1997**, *55*, 648−660.

(26) Stenholm, S. *The Foundations of Laser Spectroscopy*; Wiley: New York, 1984.

(27) Shuang, S. L. *Physics of Photonics Devices*, 2nd ed.; Wiley: New York, 2009; pp 300−307.

(28) Yariv, A. *Optical Electronics*, 4th ed.; Saunders College Publishing: Orlando, 1991; pp 519−520.

(29) Taillaert, D.; Bienstman, P.; Baets, R. *Opt. Lett.* **2004**, *29*, 2749−2751.

(30) Zhang, C.; Sun, J.-H.; Xiao, X.; Sun, W.-M.; Zhang, X.-J.; Chu, T.; Yu, J.-Z.; Yu, Y.-D. *Chin. Phys. Lett.* **2013**, *30*, 014207.

(31) Cooper, M. L.; Gupta, G.; Park, J. S.; Schneider, M. A.; Divliansky, I. B.; Mookherjea, S. *Opt. Lett.* **2010**, *35*, 784−786.

(32) Hillenbrand, R.; Keilmann, F. *Phys. Rev. Lett.* **2000**, *85*, 3029−3032.

(33) Krostowski, L.; Hochberg, M. *Silicon Photonics Design*; Cambridge University Press: Cambridge, 2015.